Boundary-Layer Meteorol (2013) 146:119–132
DOI 10.1007/s10546-012-9760-3

ARTICLE

Observations of the Early Evening Boundary-Layer Transition Using a Small Unmanned Aerial System

Timothy Bonin · Phillip Chilson · Brett Zielke · Evgeni Fedorovich

Received: 15 December 2011 / Accepted: 17 July 2012 / Published online: 2 August 2012

Abstract The evolution of the lower portion of the planetary boundary layer is investigated using the Small Multifunction Research and Teaching Sonde (SMARTSonde), an unmanned aerial vehicle developed at the University of Oklahoma. The study focuses on the lowest 200 m of the atmosphere, where the most noticeable thermodynamic changes occur during the day. Between October 2010 and February 2011, a series of flights was conducted during the evening hours on several days to examine the vertical structure of the lower boundary layer. Data from a nearby Oklahoma Mesonet tower was used to supplement the vertical profiles of temperature, humidity, and pressure, which were collected approximately every 30 min, starting 2 h before sunset and continuing until dusk. From the profiles, sensible and latent heat fluxes were estimated. These fluxes were used to diagnose the portion of the boundary layer that was most affected by the early evening transition. During the transition period, a shallow cool and moist layer near the ground was formed, and as the evening progressed the cooling affected an increasingly shallower layer just above the surface.

Keywords Early evening transition · Heat flux · Surface layer · Unmanned aerial vehicle

1 Introduction

With the rapid decline of insolation around sunset, the residual layer of the planetary boundary layer (PBL) often becomes decoupled from the surface layer under quiescent conditions. This transition period is known as the early evening transition (EET) (Acevedo and Fitzjarrald 2001), and it is marked by distinct changes at the surface and more subtle changes throughout the rest of the PBL. During this time, the PBL evolves from an unstable, convective regime to a stably stratified environment (Grimsdell and Angevine 2002). Concurrent with this, turbulence quickly decays throughout the PBL.

T. Bonin (✉) · P. Chilson · B. Zielke · E. Fedorovich
School of Meteorology and Atmospheric Radar Research Center, University of Oklahoma, Norman, OK, USA
e-mail: tim.bonin@ou.edu

Although the EET occurs to some extent on almost all evenings, it is most noticeable under clear skies and weak winds. Clear skies allow for signifcant radiational cooling of the surface (Acevedo and Fitzjarrald 2001). Additionally, strong winds induce strong turbulent mixing, often preventing the residual layer from decoupling from the surface layer. Hence, weak winds are ideal for a pronounced EET with noticeable effects on near-surface conditions.

The environmental changes that occur during the EET have important impacts on transportation and industry. During the EET, for example, there is a rapid increase in the near-surface mixing ratio, which can be sufficient for saturation later in the night (Acevedo and Fitzjarrald 2001). Therefore, the determination of whether fog will form largely depends on the magnitude of the moisture jump early during the evening. With better understanding and quantification of the surface thermodynamic changes, fog might be forecast with greater accuracy.

In addition to fog formation, there are several other consequences of the EET. The sharp near-surface cooling that occurs during the EET is an important factor for the formation of frost or freezing conditions. Frost may damage plants, resulting in large economic losses across the agricultural sector. The strong surface stability that develops in the process of the EET reduces turbulent mixing, which can cause an increase in pollutant concentrations near the ground, leading to exceedances of air quality standards. On the other hand, the formation of a low-level jet (LLJ) during the evening transition may significantly increase the amount of energy that wind turbines can produce (Sisterson and Frenzen 1978; Storm et al. 2009).

The Small Multifunction Autonomous Research and Teaching Sonde (SMARTSonde) has been developed by the Atmospheric Radar Research Center (ARRC) at the University of Oklahoma (OU) (Chilson et al. 2009). The SMARTSonde is a small unmanned aerial system (UAS) that is capable of measuring several atmospheric variables such as temperature, moisture, pressure, mean wind speed and direction, and concentrations of trace gases. A photograph of the SMARTSonde with its radio controller and ground control station (GCS) is shown in Fig. 1. The SMARTSonde has been utilized in this study to obtain sequential soundings of the lower part of the PBL, to examine how the EET affects the thermodynamic structure in this portion of the PBL.

The paper is structured as follows; in Sect. 2, a literature review of the EET and the UAS used in atmospheric research is presented. In Sect. 3, the SMARTSonde is introduced and described as a platform for PBL research. In Sect. 4, the methodology used to study the EET is discussed, and in Sect. 5 an integration method to calculate sensible and latent heat flux profiles within the PBL is introduced. In Sect. 6, the data collected during SMARTSonde flights are analyzed and discussed, detailing how the lowest 200 m of the PBL evolves during the EET. In Sect. 7 conclusions are presented.

2 Background

2.1 The Early Evening Transition

The effects of the EET are most noticeable within the first 10 m of the PBL. Fortunately, this is the portion of the atmosphere that is the easiest to access and is thus best observed. As such, the surface characteristics during the EET have been well documented (e.g. Taylor 1917; Fitzjarrald and Lala 1989; Acevedo and Fitzjarrald 2001; Bodine et al. 2009).

Around sunset, the incoming solar radiation rapidly decreases, and shortly before sunset the outgoing longwave radiation typically exceeds the incoming solar radiation, resulting in a negative net radiative flux at the surface. Consequently, the air near the surface cools,

Fig. 1 Photograph of the SMARTSonde, the radio controller, and the ground control station (GCS)

stabilizing the surface layer. As the surface layer stabilizes, turbulence rapidly decays leading to the intensification of stable stratification.

From observations near Albany, New York State, Acevedo and Fitzjarrald (2001) discovered three particular near-surface features during a strong EET. First, there is a sharp increase in specific humidity shortly before sunset, and concurrently the temperature begins to rapidly decrease. The wind gusts decrease in magnitude, which is evidence of the rapidly decaying turbulence in the surface layer. While the decrease in temperature and wind gustiness have been explained previously and are intuitive, the mechanism that increases near-surface moisture is not well understood. Fitzjarrald and Lala (1989) associated the sharp jump in moisture with turbulent moisture flux convergence into the surface layer. During the EET, the sensible heat flux at the surface is often negative (downward) while the latent heat flux is positive (upward).

During this transition period, very large spatial variations in the near-surface thermodynamic parameters develop. These heterogeneities are exacerbated by complex terrain and are largely associated with drainage flows (Shapiro and Fedorovich 2007) and differential land use. As the surface radiatively cools, the near-surface air cools as well. On slopes, this air becomes cooler than the surrounding air at the same height, resulting in negative buoyancy accelerating the air parcel down the slope. This, in addition to differential radiative cooling, is a contributing factor for the formation of cold pools that often form in valleys. It has been shown, using measurements at the Lake Thunderbird Micronet, near Norman, Oklahoma, that localized cold pools can develop with air temperatures 3–4 K lower than surrounding surface air temperatures, even when local elevation changes are as small as 6 m (Bodine et al. 2009).

While the effects of the EET may be most noticeable at the surface, the EET has an effect on the entire PBL. There have been a number of studies that have examined the transition throughout the PBL as a whole (e.g. André et al. 1978; Mahrt 1981; Grant 1997; Grimsdell and Angevine 2002). These studies have been conducted utilizing rawinsondes, tethersondes, piloted aircraft, and a wide array of numerical models. From these reports, it has been found that the middle and upper parts of the PBL exhibit a more gradual transition than the surface layer since there is no significant source of cooling other than that caused by the surface.

Typically, the boundary-layer depth remains approximately constant while the surface heat flux stays positive throughout the late afternoon (Kaimal et al. 1976; Grant 1997). However, Grimsdell and Angevine (2002) used reflectivity and Doppler spectral width from a 915-MHz wind profiler to estimate the boundary-layer depth in the afternoon and found that the convective boundary layer (CBL) shrinks on some afternoons. This occurred most often on humid days, when there was no significant capping inversion. Cumulus clouds usually developed on the days with high relative humidity when the CBL depth decreased. Grimsdell and Angevine (2002) hypothesized that a small Bowen ratio and cloudiness reducing surface heating lead to weaker thermals and a shallower mixing layer.

Although the depth of the CBL may decrease throughout the afternoon, more drastic changes do not occur until about an hour before sunset. As soon as the surface heating diminishes, the PBL decouples from the surface as mixing is inhibited between the surface and the residual layer. Since the main source for turbulence kinetic energy (TKE) is the flow interaction with the surface, TKE gradually declines through the residual layer (Grant 1997). Later in the evening, additional TKE may be generated from shear on the interface of the surface layer and the underside of a LLJ that develops during the night.

The residual layer cools at a much lower rate than the surface, and typically the rate of cooling in this layer is $\approx 0.2\,\mathrm{K\,hr^{-1}}$ (Ha and Mahrt 2003). This cooling is not the result of the turbulent heat exchange since there is no significant convective heat transport within the residual layer. Instead, most of this cooling derives from clear-air radiation (Ha and Mahrt 2003). The cooling rate is relatively constant throughout the residual layer since the clear-air radiative flux acts on the whole layer relatively uniformly. Beneath the residual layer, the cooling profile varies with height, and results from André et al. (1978) and Grant (1997) indicate a curved cooling profile (one that is not linear with height), with more drastic cooling at the surface. The curved cooling profile may be due to radiational effects (André et al. 1978) or due to the turbulent heat flux (Derbyshire 1990). Without any observations documenting the clear-air radiative flux, it is difficult to distinguish the factors that cause the curved cooling profile near the surface.

In addition to all of the thermodynamic changes in the PBL during the EET, there are often changes in the dynamics at the interface of the surface and residual layers. Particularly, at heights of a few hundred metres above the ground, a nocturnal LLJ typically forms (Mahrt 1981), and the magnitude of the increase in wind speed in the jet can reach $10–20\,\mathrm{m\,s^{-1}}$ (Wexler 1961).

2.2 Use of Unmanned Aerial Systems in Meteorological Research

The concept of using a radio-controlled aircraft to collect meteorological data is not new. Decades ago, meteorologists proposed the idea of using small airplanes to sample the atmosphere (Konrad et al. 1970). At the time, meteorological sensors were large and heavy, making it difficult to successfully mount instrumentation in a small airplane for measurements. Since then, many instruments have been designed to be small and to weigh only a few grams. With these technological advances, there has been a resurgence in efforts to create small unmanned

aircraft capable of taking atmospheric measurements. Within the past decade, there has been a handful of researchers around the world who have been developing small aircraft for atmospheric research (e.g. Holland et al. 2001; Shuqing et al. 2004; Spiess et al. 2007; Reuder et al. 2009; Elston et al. 2011).

In the early 1990s, initial research and development began for the platform design of the Aerosonde (Holland et al. 1992), the first UAS built for meteorological measurements. The system is capable of measuring temperature, humidity, pressure, trace gas concentrations, wind, and several other variables. Aerosonde flight time can be bought for research projects through the AAI Corporation, but the UAS itself cannot be purchased. Purchasing flight time for the Aerosonde makes sense for long-range missions such as the penetration of a hurricane eyewall (i.e. Lin 2006), but is not practical for routine PBL experiments that require flight times of less than an hour over short ranges.

Recently, smaller and less expensive UASs have been developed specifically to study the PBL. Spiess et al. (2007) have constructed the M^2AV platform, which is capable of measuring the turbulent three-dimensional wind vector with the use of a five-hole probe (van den Kroonenberg et al. 2008). More recently, the M^2AV has been used to calculate the structure parameter of temperature from turbulence measurements (van den Kroonenberg et al. 2012). (Reuder et al. (2009)) have developed the small unmanned meteorological observer (SUMO) for boundary-layer and arctic research. The SUMO utilizes a Paparazzi autopilot, an open-source autopilot system, for pre-configured flight patterns. The SUMO is small and lightweight, making it easily portable.

3 The SMARTSonde Platform

The initial airframe chosen for the SMARTSonde project was the NexSTAR EP Select, as used by Houston et al. (2012). As an off-the-shelf radio-controlled airplane, it was quick and easy to build on a small budget. The NexSTAR facilitated the SMARTSonde team in early training in the operation of radio-controlled airplanes while providing a robust and stable airframe. It has a 1.74 m wingspan and weighs approximately 3.5 kg. The brushless electric motor version of the NexSTAR was chosen to avoid potential contamination of the sensors from the fuel used to power a gas engine. Typical airspeed of the NexSTAR during scientific missions varies between 15–20 $m\,s^{-1}$ and flights last up to 25 min. The airplane can ascend at rates up to 2 $m\,s^{-1}$ if needed.

A Paparazzi autopilot system has been integrated into the platform (Chilson et al. 2009). The autopilot system utilizes sensors that provide data to an onboard computer to determine servo movements needed to maintain a pre-configured flight plan. Infrared sensors are used to estimate the pitch and roll of the aircraft. Concurrently, the integrated global positioning system (GPS) device built into the autopilot provides precise measurements of the position of the airplane. Based on this information relative to the flight path and the airplane's attitude, the onboard microprocessor calculates adjustments to the throttle, aileron, and elevator needed to stay on course.

The SMARTSonde is in constant communication with the ground. A pilot with a radio controller can operate the aircraft during take-offs and landings, while easily transferring control to the autopilot microprocessor with a switch. Simultaneously, the autopilot is in full-duplex communication with a GCS. Through the GCS, which is a laptop with autopilot software, the SMARTSonde's status can be monitored. Additionally, data from the meteorological sensors are relayed through the autopilot to the GCS which can be used to monitor data quality and perform basic evaluation of the data in real-time.

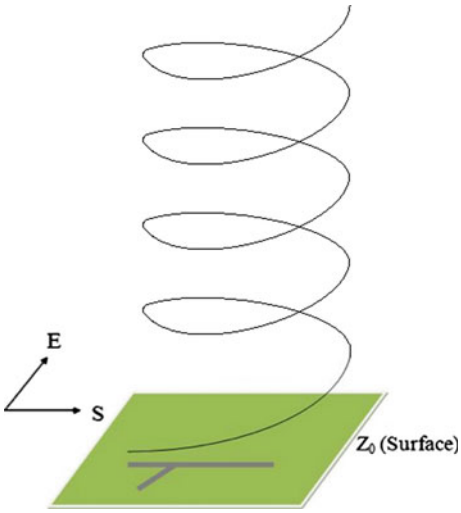

Fig. 2 In the helical flight pattern, the ascent rate is constant while the airplane circles over a small area

For the purposes of this study, two sensors were installed onto the airframe to collect the meteorological data. An SHT75 sensor by Sensirion was installed on the underside of the wing to take measurements of temperature and humidity. It uses a capacitive sensor to measure humidity while temperature is measured from a band-gap sensor. The specification sheet from Sensirion gives the response time to be 8 s and the accuracy to be within 0.3 K and 1.8 % relative humidity. The SHT75 is positioned underneath the wing near the fuselage to block direct sunlight. To further shield the sensor for short times when the plane's attitude allows sunlight underneath the wing, the SHT75 is placed in an opaque tube. An SCP1000 sensor by VTI Technologies is mounted inside of the fuselage, and is used to take accurate atmospheric pressure measurements. The SCP1000 also takes temperature measurements and internally compensates the pressure output for the fluctuations in temperature.

The two-dimensional wind vector is estimated using an algorithm that extracts the wind vector from the GPS track of the UAS, as described by Bonin et al (2011). To measure trace gas concentrations, an SM50 sensor by Aeroqual is installed inside the fuselage. The SM50 uses a fan to sample air from the environment via an intake hole in the side of the fuselage. While the SM50 can only measure one trace gas constituent at a given time, it is easy to change the gas measured by swapping the sensor chip.

4 Experimental Set-up and Meteorological Conditions

A helical ascent flight plan was developed and programmed into the airplane's autopilot patterned after the trajectory shown in Fig. 2. Using this flight plan, the airplane follows the trajectory described by a circle with a small radius of ≈60 m over a predetermined location while slowly ascending with the throttle and pitch set to constant values. If the SMARTSonde flies through an inversion, the throttle or pitch can be altered in real time so that the airplane ascends at a lower rate, thereby providing higher resolution data. Once the airplane reaches a desired maximum altitude, the motor is turned off and the airplane descends to a specified height, at which point the pilot takes control of the airplane and lands.

The flights presented in this study took place at the Central Oklahoma Radio Control Society airfield. This facility is located less than 1 km directly to the west of the National

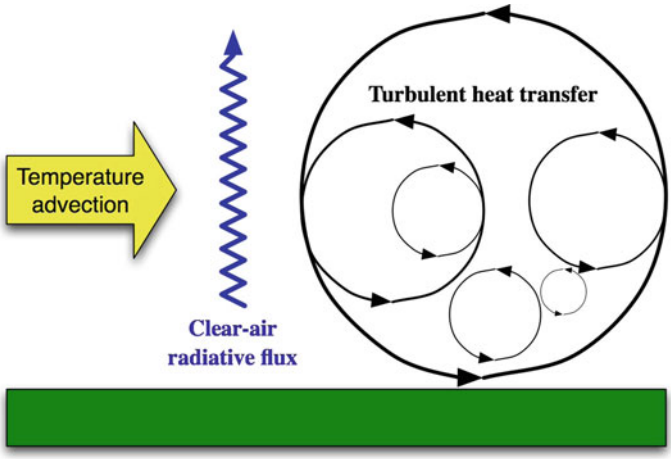

Fig. 3 Schematic of processes that affect the thermal structure of the PBL. Under certain conditions, temperature advection can be assumed to be constant through the PBL

Weather Center (NWC) in Norman, OK, USA. The close proximity of the airfield to the NWC allows for comparisons of SMARTSonde data with measurements from instrumentation on and around the NWC. In this study, data from the NWC Mesonet tower, maintained by the Oklahoma Climatological Survey, are used to complement the vertical profiles derived from SMARTSonde flights. Oklahoma Mesonet stations measure air temperature, humidity, barometric pressure, wind speed and direction, rainfall, solar radiation, and soil temperatures (Brock et al 1995; McPherson et al. 2007). The network consists of 110 sites distributed across the state.

To study how the PBL structure changes throughout the evening, flights were scheduled approximately 30 min apart to allow ample time for the environment to change. The first flight typically occurred about 90 min prior to sunset, while the last flight of the day occurred at the time of sunset. During the helical ascents, the SMARTSonde ascended at a low rate of $0.5\,\mathrm{m\,s^{-1}}$, and helped to mitigate the effect of sensor inertia by giving the temperature and humidity sensor time to adjust to the ambient conditions. Due to visibility and safety issues, the SMARTSonde was not flown after dark.

5 Estimating Heat Fluxes

An algorithm has been developed for the SMARTSonde that uses changes in temperature and humidity between two successive flights to calculate the heat flux. By applying a technique suggested by Deardorff et al. (1980), the sensible heat flux H can be estimated from consecutive temperature profiles up to a height where the heat flux can be assumed to be zero (no temperature change). The turbulent heat flux $\overline{w'\theta'}$, visualized in Fig. 3, can be evaluated by utilizing the vertically-integrated, horizontally-averaged thermodynamic equation,

$$\overline{w'\theta'}(z) = \int_{z}^{h_a} \left(\frac{\partial \theta}{\partial t} + w \frac{\partial \theta}{\partial z} \right) dz, \tag{1}$$

where θ is the potential temperature and the subscript a refers to a height where the heat flux can be assumed to be zero. Terms related to molecular diffusivity that originally appeared in the Deardorff et al. (1980) version of the above equation have been neglected, since molecular diffusion in the atmosphere is many orders of magnitude smaller than the turbulent diffusion of heat.

Under most observational conditions, the mean vertical velocity, w, can be taken as zero over flat land at the surface. Thus, with the above assumptions, Eq. 1 can be simplified as

$$\overline{w'\theta'}(z) = \int_{z}^{h_a} \frac{\partial \theta}{\partial t} dz. \tag{2}$$

The heat flux can then be calculated using the potential temperature profile obtained from the SMARTSonde, the temperature in the profile being averaged over 20-m blocks to smooth the data. Then, the averaged profile is linearly interpolated to increments of $\Delta h = 1\,\mathrm{m}$, so the integrated heat flux profile is smoother with smaller height bins. By applying finite differencing to Eq. 2 and multiplying by $c_p \rho$ to obtain the turbulent heat flux (Wm^{-2}), the following equation for the heat flux results,

$$H(z) = c_p \rho \overline{w'\theta'}(z) = \sum_{z/\Delta h}^{h_a/\Delta h} c_p \rho \frac{\Delta \theta}{\Delta t} \Delta h, \tag{3}$$

where c_p is specific heat at constant pressure, ρ is the density evaluated from temperature and pressure measurements, $\Delta\theta$ is the observed difference in potential temperature at a given height between the two flights, and Δt is the time difference in seconds between the two flights. Since finite differencing is used in the calculation of the heat flux, the calculated heat flux is more precisely an averaged heat flux over the time between the two profiles ($\approx$30 min).

Figure 3 illustrates several contributing processes that can modify the potential temperature profile in the atmosphere. In addition to the profile evolution assumed in Eq. 1, the thermal advection may be taken into account by calculating the mean potential temperature change due to advection above the PBL and subtracting this value from $\Delta\theta$ throughout the PBL, assuming the temperature advection is nearly constant with height. Based on changes in thermodynamic profiles, temperature and moisture advection appear to be independent of height for the cases in this study, so this assumption can be used. However, this method should be used with caution if vertical gradients in thermodynamic advection are large (e.g. in a LLJ scenario). The adopted integration approach also assumes that the clear-air radiative flux is negligible or constant throughout the PBL. Overall it provides a valid method to estimate the heat flux using temperature profiles obtained with SMARTSonde.

As with H, the latent heat flux F can be estimated as:

$$F = \sum_{z/\Delta h}^{h_a/\Delta h} \lambda \rho \frac{\Delta q}{\Delta t} \Delta h, \tag{4}$$

where λ is the latent heat of vaporization ($2.5 \times 10^6\ \mathrm{J\,kg^{-1}}$), and Δq is the change in the specific humidity at a particular height.

To the authors' knowledge, this is the first time that such an approach has been used to estimate sensible and latent heat fluxes in the atmosphere from UAS measurements.

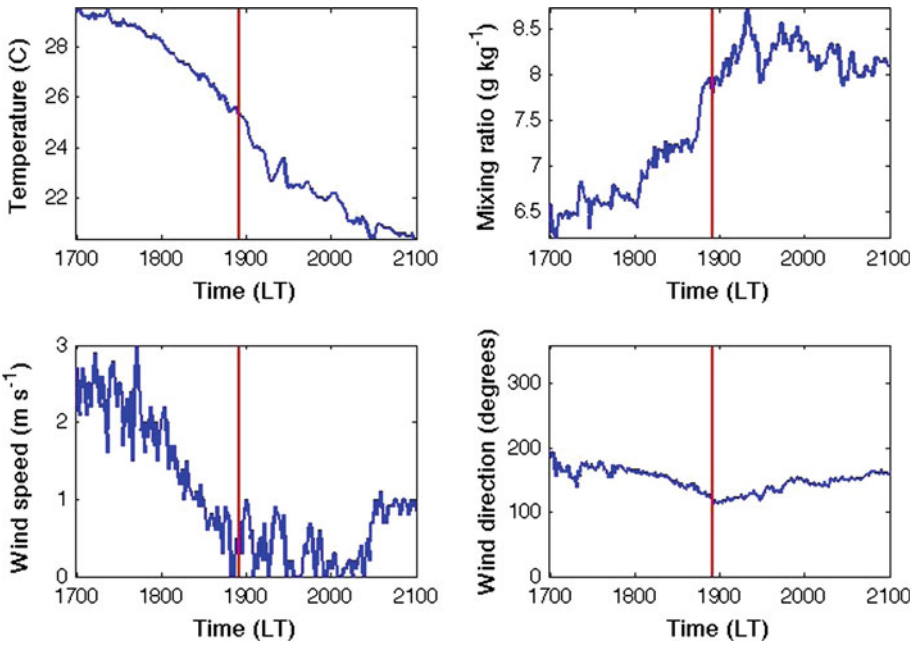

Fig. 4 Data from the NWC Mesonet site for October 15, 2010 given in local time (LT). The *red line* denotes astronomical sunset

6 SMARTSonde Observations of the EET

To better understand how the thermodynamic structure of the PBL evolves during the early evening transition (EET), the SMARTSonde flew sequential flights throughout the EET over the lowest 200 m a.g.l. on five occasions over a time period from October 2010 to February 2011. Results from two of those days are presented in this study since three to four successful flights occurred on each of the days. Temperature and moisture advection was negligible during the first day, but was important during the second day.

Optimal weather conditions for SMARTSonde flights are also favorable for the occurrence of pronounced EET events. Light winds, clear skies, weak synoptic scale forcing constitute ideal flying conditions that also promotes clear transition periods (Acevedo and Fitzjarrald 2001). In both cases considered, the surface winds were weak and the skies were mostly cloudless, allowing for strong radiational cooling. Additionally, there were no surface boundaries or strong weather systems nearby on both days.

6.1 October 15, 2011 EET

The first case presented is from October 15, 2010, during which the EET surface changes and ambient synoptic conditions were very similar to those described by Acevedo and Fitzjarrald (2001). The surface moisture displayed a very rapid jump shortly before sunset. Additionally, the surface winds became less gusty and the wind speed rapidly decreased during the observation time frame (see Fig. 4).

Even though sunset was at 1857 local standard time (LST), the EET appears to have already begun by the time of the first flight at 1721 LST. The layer of air near the surface had

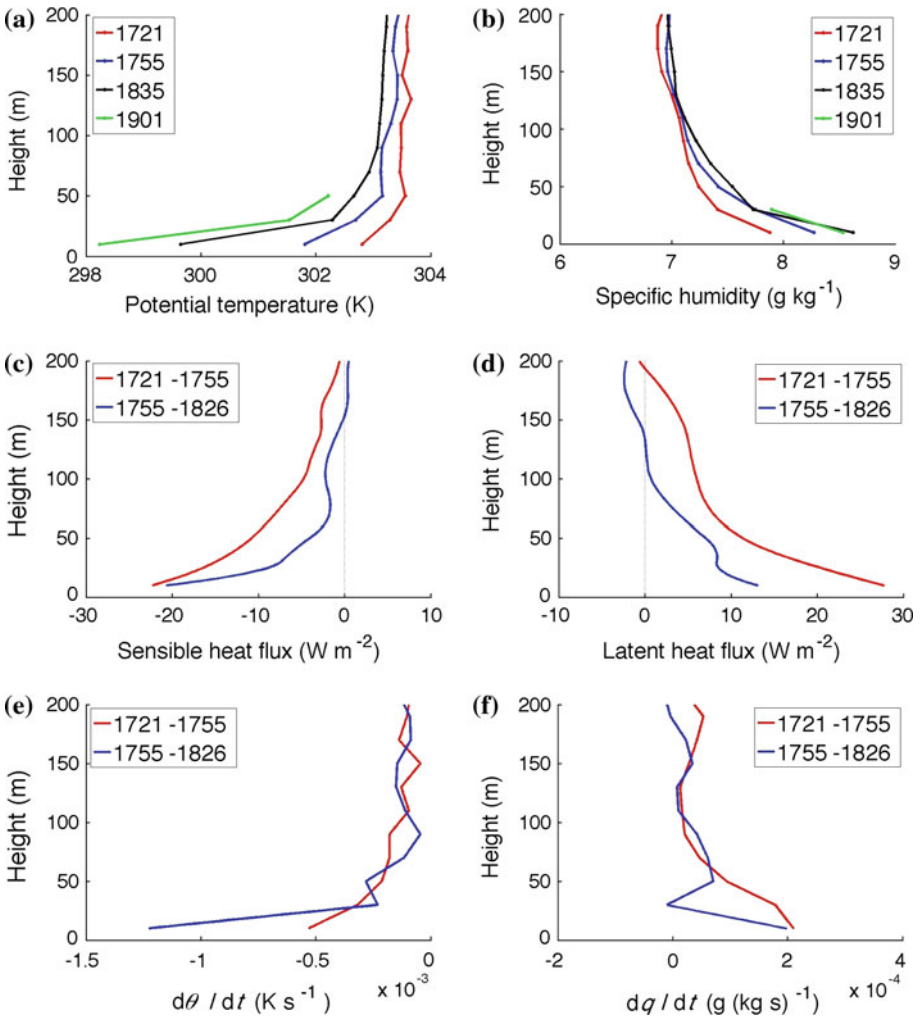

Fig. 5 **a** Potential temperature, **b** specific humidity, **c** sensible heat flux, **d** latent heat flux, **e** warming rate, and **f** moisture change from SMARTSonde flights on the evening of October 15, 2010. Times of flights are given in local time

already become stable, as evidenced by the 40-m deep inversion in Fig. 5a. This observation is also supported by the fact that the near-surface temperature reported by the Mesonet station began to decrease at about this time. The cooling continued to accelerate over the next couple of hours. A dramatic cooling took place over a shallow layer just above the surface, as can be seen from the sensible heat flux profiles in Fig. 5c. The cooling rate profile is notably curved, as the cooling rate is largest at the surface and its magnitude quickly decreases with height. The curved cooling profile was also observed in the past studies of the EET by André et al. (1978) and Grant (1997).

While the surface sensible heat flux becomes negative for the first hour of the EET, the surface latent heat flux remains positive during that period. This agrees with the data given by Fitzjarrald and Lala (1989). The noticeable positive latent heat flux is in a fairly shallow

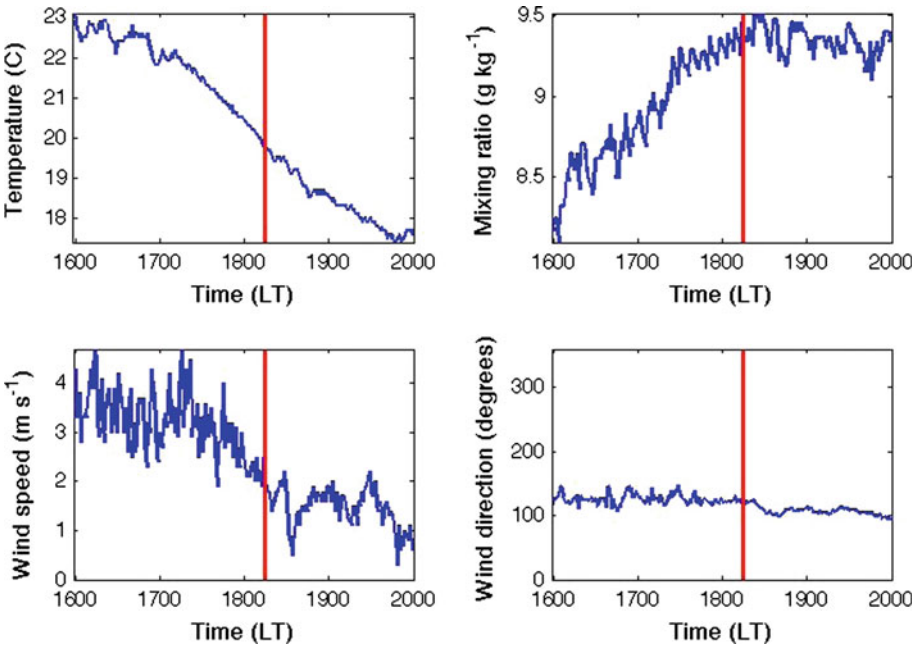

Fig. 6 Same as Fig. 4, for February 18, 2011

layer near the surface, implying that the moisture is transported upwards through a very small portion of the PBL during the transition.

6.2 February 18, 2011 EET

The second case, which was observed on February 18, 2011, although exhibits characteristic features of the EET, but these features are not as explicit as those observed in the previous case. On this day, the surface winds were again fairly light, as can be seen from the NWC Mesonet site data shown in Fig. 6. The surface observations indicate a decrease in temperature and increase in moisture, which are expected during an EET. However, the moisture increased several hours prior to sunset, before the EET could affect the moisture field. An analysis of the corresponding synoptic conditions reveals that there was cold and moist air advection to the area. In addition to local sensible and latent heat fluxes, advection was partially responsible for cooling and moistening of the near-surface air during the EET. The advection can be seen to affect the entire 200-m range of heights above the surface by altering the full extent of the profiles in Fig. 7. By averaging the cooling rate at all heights over 150 m, above which turbulent transport can assumed to be negligible, the mean rate of cooling from temperature was found to be $\approx 0.9\,\mathrm{K\,h^{-1}}$ between the first two flights and $\approx 1.25\,\mathrm{K\,h^{-1}}$ between the second and third flight. Assuming height-constant advection, the heat flux was calculated after removing the influence of advection on the cooling profile.

The first flight on February 18, which occurred about two hours prior to sunset, took place while the PBL was still very convective (unstable). This is indicated, in particular, by the superadiabatic layer near the surface in Fig. 7a. Even though the first flight started under convective conditions, the mean surface heat flux between the first two flights was negative as the surface started to cool. This negative heat flux is reflected by the strong cooling in the lowest 70 m, as the near-surface portion of the PBL becomes much more stable. Once again,

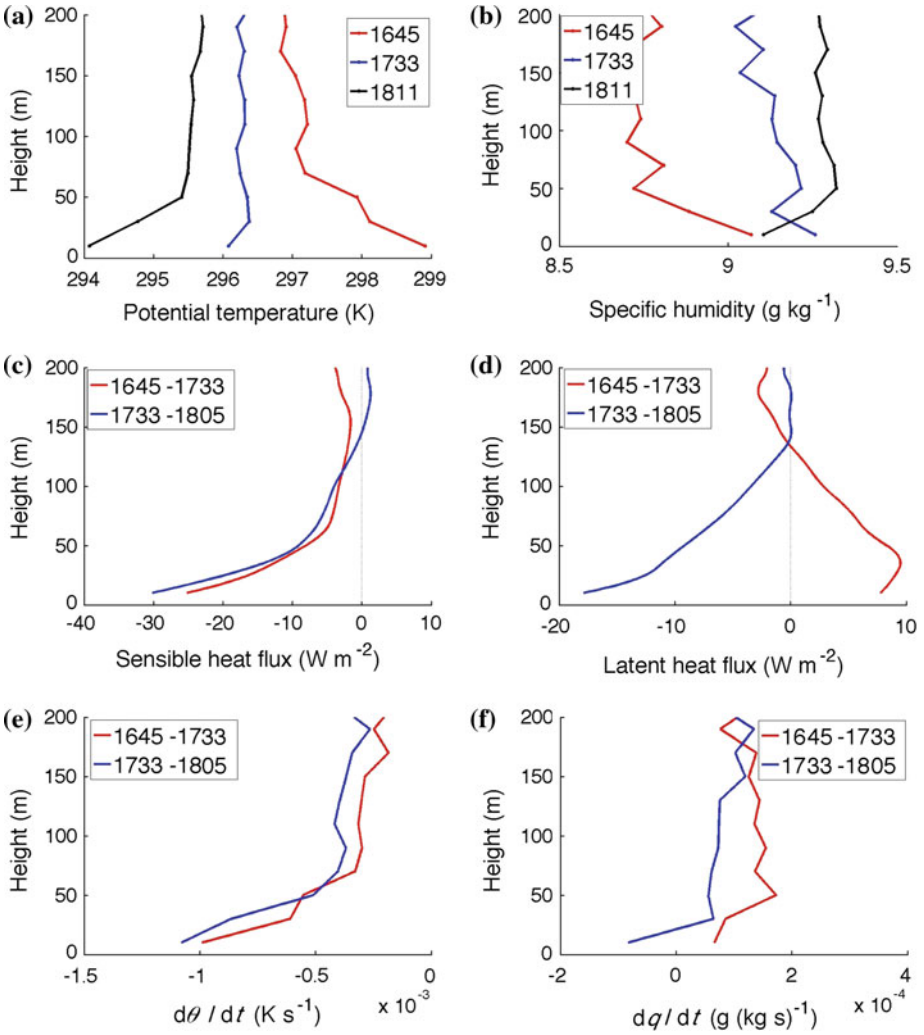

Fig. 7 Same as Fig. 5, except for EET on February 18, 2011

as the evening proceeded, the cooling took place over a progressively shallower layer. This is shown in Fig. 7c, as the majority of the cooling between 1645 and 1733 was below 70 m while it was mostly below 50 m between 1733 and 1805.

On this particular day, the latent heat flux was positive early in the evening but became negative as sunset approached. This differs from the October 15 case, when the latent heat flux remained positive closer to sunset. To some extent, this difference could be a result of a violated assumption of the moisture advection being constant with height.

7 Summary and Conclusions

Since 2009, the SMARTSonde has been in development by the Atmospheric Radar Research Center at the University of Oklahoma, and it has been used to measure consecutive profiles

of meteorological variables in the PBL during afternoon and early evening hours. On each day, three or four flights took place, beginning about two hours before sunset to capture the entirety of the EET. To better examine the temporal changes in near-surface conditions during the EET, measurement data from the NWC Mesonet tower were used to complement the profiles measured with the SMARTSonde.

Out of 5 days the EET was observed, two cases were selected for analysis. In the first case, the winds were light and became weaker throughout the evening. The conditions were ideal for a pronounced EET, evidenced by the sharp increase in moisture and decrease in temperature. The second case was similar, except that there was some significant cool, moist air advection in place during the time of the flights.

With vertical profiles of temperature and humidity measured by the SMARTSonde, it is possible to identify the vertical extent of the PBL portion that is mostly affected by the EET. Additionally, it is possible to identify flow regions where sensible and latent heat fluxes have opposite signs. As the evening advances, the cooling was found to occupy a progressively narrower layer near the surface. This is apparently due to the suppression of vertical turbulence by the increasing stability past the EET. As the surface cooled, there was still a positive latent heat flux near the surface during the early part of the transition. This observation agrees with the previous study of Acevedo and Fitzjarrald (2001). During the later stages of the EET, the latent heat flux decreased as turbulent exchange between the land surface and the atmosphere diminished greatly.

Acknowledgements We thank our colleagues who have helped with the collection of the data, including all of those who assisted in the development of the SMARTSonde. We are especially thankful for Wayne Shalamunec for assisting in the development and piloting the SMARTSonde, and to the CORCS for allowing use of the airfield for flights. Funding to support the development of SMARTSonde has been provided by the University of Oklahoma (OU) Atmospheric Radar Research Center (ARRC) and through a grant provided by the National Oceanic Atmospheric Administration (NOAA) National Severe Storms Laboratory (NSSL).

References

Acevedo OC, Fitzjarrald DR (2001) The early evening surface-layer transition: temporal and spatial variability. J Atmos Sci 58:2650–2667

André J, De Moor G, Lacarrére P, Therry G, Du Vachat R (1978) Modeling the 24-hour evolution of the mean and turbulent structures of the planety boundary layer. J Atmos Sci 35:1861–1883

Bodine D, Klein PM, Arms SC, Shapiro A (2009) Variability of surface air temperature over gently sloped terrain. J Appl Meteorol Climatol 48:1117–1141

Bonin T, Zielke B, Bocangel W, Shalamunec W, Chilson PB (2011) An analysis of wind retrieval algorithms for small unmanned aerial systems. In: 91st American Meteorological Society Annual Meeting, Seattle, WA, USA

Brock FV, Crawford KC, Elliott RL, Cuperus GW, Stadler SJ, Johnson HL, Eilts MD (1995) The oklahoma mesonet: A technical overview. J Atmos Ocean Technol 12:5–19

Chilson PB, Gleason A, Zielke B, Nai F, Yeary M, Klein PM, Shalamunec W (2009) SMARTSonde: a small UAS platform to support radar research. In: 34th Conference on radar meteorology, American Meteorological Society. Extended abstract 12B.6, Boston. http://ams.confex.com/ams/34Radar/techprogram/paper_156396.htm

Deardorff J, Willis G, Stockton B (1980) Laboratory studies of the entrainment zone of a convectively mixed layer. J Fluid Mech 100:41–64

Derbyshire SH (1990) Nieuwstadt's stable boundary layer revisited. Q J R Meteorol Soc 116:127–158

Elston JS, Roadman J, Stachura M, Argrow B, Houston A, Frew E (2011) The tempest unmanned aircraft system for in situ observations of tornadic supercells: design and VORTEX2 flight results. J Field Robotics 28:461–483

Fitzjarrald DR, Lala G (1989) Hudson valley fog environments. J Appl Meteorol 28:1303–1328

Grant AM (1997) An observational study of the evening transition boundary-layer. Q J R Meteorol Soc 123:657–677

Grimsdell AW, Angevine WM (2002) Observations of the afternoon transition of the convective boundary layer. J Appl Meteorol 41:3–11
Ha KJ, Mahrt L (2003) Radiative and turbulent fluxes in the nocturnal boundary layer. Tellus 55:317–327
Holland G, Webster P, Curry J, Tyrell G, Gauntlett D, Brett G, Becker J, Hoag R, Vaglienti W (2001) The aerosonde robotic aircraft: a new paradigm for environmental observations. Bull Am Meteorol Soc 82:889–901
Holland GJ, McGeer T, Youngren H (1992) Autonomous aerosondes for economical atmospheric soundings anywhere on the globe. Bull Am Meteorol Soc 73:1987–1998
Houston A, Argrow B, Elston JS, Lahowetz J, Frew E, Kennedy PC (2012) The collaborative Colorado–Nebraska unmanned aircraft system experiment. Bull Amer Meteor Soc 93:39–54
Kaimal JC, Wyngaard JC, Haugen DA, Cote OR, Izumi Y, Caughey S, Readings CJ (1976) Turbulence structure in the convective boundary layer. J Atmos Sci 33:2152–2169
Konrad T, Hill M, Rowland R, Meyer J (1970) A small, radio-controlled aircraft as a platform for meteorological sensors. Johns Hopkins APL Tech Dig 10:11–19
Lin PH (2006) Observations: the first successful typhoon eyewall-penetration reconnaissance flight mission conducted by the unmanned aerial vehicle, aerosonde. Bull Am Meteorol Soc 87:1481–1483
Mahrt L (1981) The early evening boundary layer transition. Q J R Meteorol Soc 107:329–343
McPherson RA, Fiebrich CA, Crawford KC, Kilby JR, Grimsley DL, Martinez JE, Basara JB, Illston BG, Morris DA, Kloesel KA, Melvin AD, Shrivastava H, Wolfinbarger JM, Bostic JP, Demko DB, Elliott RL, Stadler SJ, Carlson J, Sutherland AJ (2007) Statewide monitoring of the mesoscale environment: A techincal update on the Oklahoma Mesonet. J Atmos Ocean Technol 24:301–321
Reuder J, Brisset P, Jonassen M, Müller M, Mayer S (2009) The small unmanned meteorological observer SUMO: a new tool for atmospheric boundary layer research. Meteorol Z 18:141–147
Shapiro A, Fedorovich E (2007) Katabatic flow along a differentially cooled sloping surface. J Fluid Mech 571:149–175
Shuqing M, Hongbin C, Gai W, Yi P, Qiang L (2004) A miniature robotic plane meteorological sounding system. Adv Atmos Sci 21:890–896
Sisterson DL, Frenzen P (1978) Nocturnal boundary-layer wind maxima and the problem of wind power assessment. Environ Sci Technol 12:218–221
Spiess T, Bange J, Buschmann M, Vörsmann P (2007) First application of the meteorological Mini-UAV' M^2AV'. Meteorol Z 16:159–169
Storm B, Dudhia J, Basu S, Swift A, Giammanco I (2009) Evaluation of the weather research and forecasting model on forecasting low-level jets: implications for wind energy. Wind Energy 12:81–90
Taylor GI (1917) The formation of fog and mist. Q J R Meteorol Soc 43:241–268
van den Kroonenberg A, Martin T, Buschmann M, Bange J, Vorsmann P (2008) Measuring the wind vector using the autonomous mini aerial vehicle M^2AV. J Atmos Ocean Technol 25:1969–1982
van den Kroonenberg A, Martin S, Beyrich F, Bange J (2012) Spatially-averaged temperature structure parameter over a heterogeneous surface measured by an unmanned aerial vehicle. Boundary-Layer Meteorol 142:55–77. doi:10.1007/s10546-011-9662-9
Wexler H (1961) A boundary layer interpretation of the low-level jet. Tellus 13:368–378